Available online at www.sciencedirect.com
ScienceDirect
International Journal of Heat and Mass Transfer 49 (2006) 5035–5048
International Journal of HEAT and MASS TRANSFER
www.elsevier.com/locate/ijhmt

The second largest Lyapunov exponent and transition to chaos of natural convection in a rectangular cavity

Hideshi Ishida [a,*], Shojiro Kawase [b], Hideo Kimoto [a]

[a] *Department of Mechanical Science and Bioengineering, Graduate School of Engineering Science, Osaka University, 1-3 Machikaneyama, Toyonaka, Osaka 560-8531, Japan*
[b] *Hayashi Telempu Co., Ltd., 1-4-5 Kamimaezu, Naka-ku, Nagoya 460-0013, Japan*

Received 9 July 2004; received in revised form 17 June 2005
Available online 25 September 2006

Abstract

In this study we have proposed an accurate and simple method to evaluate the Lyapunov spectrum. The method is suitable for any discretization method that finally expresses a governing equation system in the form of an ordinary differential equation system. The method was applied to evaluate up to the second largest Lyapunov exponents for natural convection in a rectangular cavity with heated and cooled side walls. The main results are as follows: (1) the largest and second largest Lyapunov exponents can be evaluated without any parameters that affects the exponents. (2) The second largest Lyapunov exponent makes it possible to classify quantitatively thermal convection fields into five regimes against the Rayleigh number and to clarify the transition route from steady state to chaos by identifying the first and second Hopf bifurcations. (3) The fluctuation in thermal convection fields just over the critical Rayleigh number at which Hopf bifurcation occurs can be quantitatively explained by using normalized Lyapunov vectors, associated with the computation of the Lyapunov exponents, just under the critical point.

Keywords: Natural convection; Rectangular cavity; Numerical analysis; Chaos; Lyapunov spectrum; Lyapunov vector

1. Introduction

Transition to natural convection in a vertical cavity with heated and cooled vertical side walls has been the subject of many research papers. In most of these studies transitions such as from unicellular flow to multicellular flow were viewed as boundary-value problems and were intended to be explained using bifurcation diagrams [1] of several (steady) solutions under the given boundary condition whose stability was determined by linear [2] or weak nonlinear analyses [3]. Once the flows lose their stability and become unsteady flows, however, the same analyses are not applicable to the change of flow regime in unsteady flows including chaos or turbulent flows except periodic ones [4], because these flows have strong nonlinearity with regard to stretching and folding action in addition to their unsteadiness.

Because of the above-mentioned reasons there is very little work available on the unsteady characteristics [5,6], including chaotic ones [7,8], of thermal convection fields. Ishida et al. [9] experimentally examined thermal convection fields in a tall cavity and found that significant chaotic temperature fluctuation exists in the region of secondary cellular flow. Ishida et al. [10] also quantitatively classified the unsteady region of a wall plume adjacent to a vertical side wall with an embedded line heat source into periodic and chaotic regions and, consequently, showed four flow regimes in the flow direction. Similar relationships between flow regimes and their chaotic properties were determined numerically in a vibrated thermal convection field in a square enclosure [11].

* Corresponding author. Tel.: +81 6 6850 6162; fax: +81 6 6850 6161.
E-mail address: ishida@me.es.osaka-u.ac.jp (H. Ishida).

0017-9310/$ - see front matter © 2005 Elsevier Ltd. All rights reserved.
doi:10.1016/j.ijheatmasstransfer.2005.06.046

Nomenclature

a	thermal diffusivity [m^2/s]
CC	convergence criterion
(C)	chaotic flow regime
c_ζ	complex form of Fourier coefficient of vorticity
$c_{\zeta_2'}$	complex form of Fourier coefficient of vorticity component of the second Lyapunov vector
D	dimension
f	frequency
Gr	Grashof's number ($=g\beta\Theta L^3/\nu^2$)
g	acceleration due to gravity [m/s^2]
J	Jacobian
k	thermal conductivity [J/(ms °C)], local kinetic energy
L	width of cavity, representative length [m]
Nu	surface-averaged Nusselt's number
NP	number of definition points
(P)	periodic flow regime
(p1)–(p5)	reference point No. 1–5, defined in Table 3
Q	local enstrophy
(QP)	quasi-periodic flow regime
Pr	Prandtl's number ($=\nu/a=0.71$)
Ra	Rayleigh's number ($=PrGr$)
(S)	steady flow regime
T	dimensioned temperature [°C]
$T^{\Delta t}$	Δt-evolution operator
t	dimensionless time
u	x velocity component
v	y velocity component
X	dimensioned X coordinate [m]
x	dimensionless X coordinate
Y	dimensioned Y coordinate [m]
y	dimensionless Y coordinate

Greek symbols

α	aspect ratio
β	thermal expansion coefficient [1/°C]
χ	eigenvalue
Δt	time step
Δx	spatial increment in the x direction
Δy	spatial increment in the y direction
ϕ	general quantity
φ	dimensionless stream function
θ	dimensionless temperature ($=(T-T_c)/\Theta$)
Θ	representative temperature difference ($=T_h-T_c$) [°C]
$\varepsilon, \varepsilon_2$	proportional constant
λ_i	ith largest Lyapunov exponent
ν	kinetic viscosity [m^2/s]
τ	period, representative time scale ($\approx\alpha^{1/2}PrRa^{-1/2}$)
ζ	dimensionless vorticity
ζ_1'	dimensionless vorticity component of the first Lyapunov vector

Subscripts

amp	amplitude
c	cooled side wall, critical value
h	heated side wall
s	steady state
θ	temperature
0	zeroth or initial value

In these analyses the largest Lyapunov exponent, which is the indicator of the sensitive dependence of initial conditions, was utilized to quantify the chaotic characteristics. However the computation of the indicator, proposed by Wolf et al. [12], is based on the embedding technique [13] and involves the physically relevant determination of the values of such parameters as embedding dimension, delay time, etc. on which the indicator depends. The resolution of the problem is impossible for the case of experimental data analyses, whereas it is possible for numerical analyses in which entire flow fields are solved. To our knowledge, Bruneau and Saad [14] were the first to obtain the largest Lyapunov exponent for a steady thermal convection field in a rectangular cavity with aspect ratio of 8 by using the formulation of a linear analysis without the embedding technique, and obtained the critical Rayleigh number for the flow to be periodic.

In this study an accurate method to compute the Lyapunov spectrum of thermal convection fields, which generalizes the concept of the largest Lyapunov exponent, is proposed by the formulation of linear analyses. The method does not involve the determination mentioned above and makes it possible to obtain the Lyapunov spectrum by, in principle, the same method as for any numerical solution including steady, periodic and chaotic ones. The spectrum not only provides the quantitative measure for unsteady solutions but also has an important property relating to the Kaplan–Yorke dimension [15] and Kolmogorov entropy (Pesin's identity [16]), and it characterizes nonequilibrium dynamics. In this study the method was applied to compute up to the second largest Lyapunov exponent and to obtain various critical Rayleigh numbers. Consequently the transition from steady to unsteady flow was quantitatively analyzed and the transition route to chaos was clarified. Moreover, the fluctuations of physical quantities over the critical number are shown to be explained by the physical quantities associated with the Lyapunov spectrum under the critical number. The proposed computational method for the Lyapunov spectrum just requires several times the amount of computational time and storage over what is needed for the conventional computation of flow field, and is very useful for many applications.

2. Methods and definitions

2.1. Physical model and governing equations

The physical model and the coordinate definition of this study are shown in Fig. 1. The thermal convection field in an enclosure was assumed to be uniform in the direction normal to the figure, and a two-dimensional coordinate system is fixed on the enclosure. Y coordinate is defined as the inverse direction of gravity along the left hand side wall and X coordinate is defined as the direction normal to the Y-axis along the bottom wall, as shown in Fig. 1. The origin is at the lowest left corner of the enclosure. The width of the enclosure is L and the height is L times the aspect ratio α. The left hand side wall shown in Fig. 1 is heated to T_h and the right hand side wall is cooled to T_c. The top and bottom walls are adiabatic. The velocity component on the wall surface is 0. Initially the fluid in the enclosure is stationary and is at temperature T_c.

On the assumption that the physical properties of the fluid are almost constant, the Boussinesq approximation can be applied to the governing equations. The normalized basic equations are given as follows:

$$u = \frac{\partial \varphi}{\partial y}, \quad v = -\frac{\partial \varphi}{\partial x}, \quad \nabla^2 \varphi = -\zeta, \tag{1}$$

$$\frac{\partial \zeta}{\partial t} + \frac{\partial (u\zeta)}{\partial x} + \frac{\partial (v\zeta)}{\partial y} = Gr \frac{\partial \theta}{\partial x} + \Delta \zeta, \tag{2}$$

$$\frac{\partial \theta}{\partial t} + \frac{\partial (u\theta)}{\partial x} + \frac{\partial (v\theta)}{\partial y} = \frac{1}{Pr} \Delta \theta, \tag{3}$$

where φ and ζ are the dimensionless stream function and vorticity, respectively. They were normalized by the representative length L, representative temperature difference Θ ($=T_h - T_c$) and kinetic viscosity ν. Gr and Pr are the Grashof number and the Prandtl number based on L and Θ, respectively. In the following, Pr was held constant at 0.71 and the Rayleigh number Ra ($=GrPr$) was varied between 0.1 and 10^7. The aspect ratio α was basically held constant at 5 except in the case of comparison with a benchmark solution, described in Section 3.

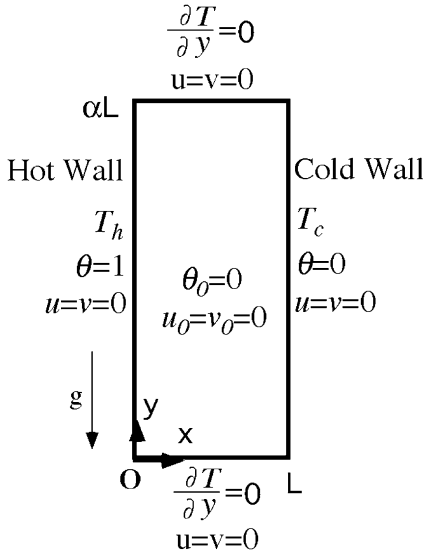

Fig. 1. Physical model and coordinate definition.

These basic equations were discretized by a finite volume method. The QUICK scheme and the second order central difference scheme were applied to convection terms and diffusion terms, respectively. For time evolution the explicit method was used. The spatial increments Δx and Δy were 1/80 and 1/40, respectively. The time step Δt decreases from 10^{-5} to 10^{-6} with increasing Ra so that the stability condition of the above-mentioned difference scheme would be satisfied. This Δt ($<10^{-5}$) is too small only for the satisfaction of the condition in some cases of small Ra. However it is responsible for sufficient accuracy of computed Lyapunov exponents as mentioned below. The convergence criterion for the Poisson equation (1) was that the maximum relative residual of φ was less than $CC = 1.0 \times 10^{-7}$. These computations, including the evaluation of Lyapunov exponents mentioned below, were performed in double precision.

In general the computed physical quantities are time-dependent. And so the statistically steady state in which the fluctuation of each physical quantity follows a steady distribution was defined as a "quasi-steady state", and the characteristics of thermal convection fields were examined in such a state.

2.2. The Lyapunov spectrum

In experiments, we usually have the time-variation data of limited variables at limited points. In this respect the conventional method based on the embedding technique, proposed by Takens [13], is useful to compute the largest Lyapunov exponent [12] or Lyapunov spectrums [17] from such experimental data. However the technique involves the determination of optimal values of such parameters as embedding dimension, delay time, evolution time, etc., and the computed exponents tend to fluctuate around these optimal values [9–11]. Moreover the distance from a reference trajectory to a neighboring (nearby) one, required to evaluate the stretching rate, should be essentially infinitesimal and, therefore, the evaluation from non-zero distance in the technique inevitably involves numerical errors. In this study we present an accurate and simple method to evaluate the exponents for the thermal convection fields suitable for numerical computations. This is based on the standard method that has been applied to ordinary differential equation systems [18–21].

Now let us consider an ordinary differential equation system. Assuming the governing equations of the system can be expressed as $d\boldsymbol{\phi}/dt = \boldsymbol{v}(\boldsymbol{\phi})$ ($\boldsymbol{\phi} = (\phi_1, \phi_2, \ldots, \phi_D)$; D: dimension), we have the governing equations of infinitesimal perturbation vector (tangent vector) $\boldsymbol{\phi}'$ as follows:

$$\frac{d\boldsymbol{\phi}'}{dt} = J(t)\boldsymbol{\phi}', \quad J_{ij} \equiv \frac{\partial v_i}{\partial \phi_j}. \tag{4}$$

This is an ordinary linear differential equation system and J(t), the Jacobian, is evaluated along a referential trajectory. From Eq. (4) we can obtain a fundamental matrix Λ and its eigenvalues $\chi_i(t)$ ($i = 1,2,\ldots,D$). Then the Lyapunov exponents can be expressed as follows [22]:

$$\lambda_i = \lim_{t\to\infty} \frac{1}{t} \ln|\chi_i(t)|. \tag{5}$$

Providing $\lambda_1 \geqslant \lambda_2 \geqslant \cdots \geqslant \lambda_D$, and where the largest Lyapunov exponent λ_1 corresponds to: (1) the real part of the largest eigenvalue obtained from the linear stability analysis for a steady solution $\boldsymbol{v}(\phi) = \boldsymbol{0}$ ($\lambda_1 < 0$), (2) the real part of the largest Floquet exponent [23] for a periodic solution $\boldsymbol{\phi}(t+T) = \boldsymbol{\phi}(t)$ ($\lambda_1 = 0$), and (3) the so-called largest Lyapunov exponent in the field of chaotic theory. The largest Lyapunov exponent is the indicator of the sensitive dependence of initial conditions, and dynamical systems with $\lambda_1 > 0$ are widely accepted and defined to be chaotic. Moreover, by computing λ_2, we can distinguish two torus ($\lambda_1 = \lambda_2 = 0$) from stable limit cycle ($\lambda_1 = 0 > \lambda_2$). Therefore Lyapunov exponents can provide unified measures to determine the condition of systems, not limited to chaotic ones. The above discussion is based on the fact that the real parts of the eigenvalues of the stability matrix equal the corresponding Lyapunov exponents [20].

Applying the power method [24], we can obtain the largest Lyapunov exponent for almost all initial conditions of $\boldsymbol{\phi}'_1$ as follows:

$$\lambda_1 = \lim_{t\to\infty} \frac{1}{t} \ln\left|\boldsymbol{\phi}'_1(t)\right|. \tag{6}$$

In this study $\boldsymbol{\phi}'_1$ is referred to as the first Lyapunov vector [21].

The second largest Lyapunov exponent is similarly computed by using the Gram–Schmidt orthogonalization technique (GSO) as follows [12,19–21]:

$$\lambda_2 = \lim_{\Delta t\to 0}\left(\lim_{N\to\infty} \frac{1}{N\Delta t} \ln|\hat{\boldsymbol{\phi}}'_2(N)|\right), \tag{7}$$

such that

$$\hat{\boldsymbol{\phi}}'_1(i+1) = T^{\Delta t}\hat{\boldsymbol{\phi}}'_1(i),$$
$$\hat{\boldsymbol{\phi}}'_2(i+1) = T^{\Delta t}\hat{\boldsymbol{\phi}}'_2(i) - (T^{\Delta t}\hat{\boldsymbol{\phi}}'_2(i)\hat{\boldsymbol{\phi}}'_1(i+1)) \times \hat{\boldsymbol{\phi}}'_1(i+1)/|\hat{\boldsymbol{\phi}}'_1(i+1)|^2,$$

where

$$\hat{\boldsymbol{\phi}}'_1(i) \equiv \boldsymbol{\phi}'_1(t_0 + i\Delta t), \quad \hat{\boldsymbol{\phi}}'_2(i) \equiv \boldsymbol{\phi}'_2(t_0 + i\Delta t), \quad \boldsymbol{\phi}'_1(t_0)\cdot\boldsymbol{\phi}'_2(t_0) = 0,$$

and $T^{\Delta t}$ is Δt-evolution operator, which is given by the integration of Eq. (4). Similarly $\boldsymbol{\phi}'_2$ is referred to as the second Lyapunov vector [21]. In Eq. (7) the limit on N should be performed before we take the limit on Δt. Actually the limit on Δt is not necessary when Δt is sufficiently small. In this study the limit could be omitted because Δt is, in consequence, sufficiently smaller than $1/|\lambda_1|$ or $1/|\lambda_2|$. The third or higher Lyapunov exponents are similarly obtained by using the GSO algorithm. GSO algorithm is utilized so that all of the Lyapunov vectors do not converge to the most amplified vector, i.e., the first Lyapunov vector. Thus we have the full spectrum of Lyapunov exponents. It should be noted that such an evaluation (Eqs. (6) and (7)) does not involve the determination or numerical errors mentioned above.

When we use the finite volume method to solve the governing equations (1)–(3), their discretized equations can be regarded as an ordinary differential equation system and, therefore, the same method can be applied to evaluate the Lyapunov exponents. In this case the vector ϕ can be expressed by $\boldsymbol{\phi} = (\zeta_1, \zeta_2, \ldots, \zeta_{\mathrm{NP}}, \theta_1, \theta_2, \ldots, \theta_{\mathrm{NP}})$, where NP is the number of definition points, because u, v and φ are considered the functions of ζ and θ. If any physical quantity ϕ of thermal convection fields is divided into a referential value $\phi^{(0)}$ and its infinitesimal perturbation (tangent vector) ϕ', such a perturbation is governed by the following linearized equations:

$$u' = \frac{\partial\varphi'}{\partial y}, \quad v' = -\frac{\partial\varphi'}{\partial x}, \quad \nabla^2\varphi' = -\zeta', \tag{8}$$

$$\frac{\partial\zeta'}{\partial t} + \frac{\partial(u^{(0)}\zeta')}{\partial x} + \frac{\partial(v^{(0)}\zeta')}{\partial y} + \frac{\partial(u'\zeta^{(0)})}{\partial x} + \frac{\partial(v'\zeta^{(0)})}{\partial y} = Gr\frac{\partial\theta'}{\partial x} + \Delta\zeta', \tag{9}$$

$$\frac{\partial\theta'}{\partial t} + \frac{\partial(u^{(0)}\theta')}{\partial x} + \frac{\partial(v^{(0)}\theta')}{\partial y} + \frac{\partial(u'\theta^{(0)})}{\partial x} + \frac{\partial(v'\theta^{(0)})}{\partial y} = \frac{1}{Pr}\Delta\theta'. \tag{10}$$

The boundary condition of a perturbation ϕ' is identical with its referential value $\phi^{(0)}$ except $\theta'_{\mathrm{h}} = \theta'_{\mathrm{c}} = 0$. In discretizing equations (8)–(10), we have the operator $T^{\Delta t}$ of a tangent vector $\boldsymbol{\phi}' = (\zeta'_1, \zeta'_2, \ldots, \zeta'_{\mathrm{NP}}, \theta'_1, \theta'_2, \ldots, \theta'_{\mathrm{NP}})$ mentioned above. It is worthwhile noting that the discretization of the 4th and 5th term on the left hand side of Eqs. (9) and (10) should be performed by the upstream interpolation referring to the flow direction not of u' and v' but of $u^{(0)}$ and $v^{(0)}$. Because the governing equation of the tangent vector should be Eq. (4); the discretization of Eqs. (1)–(3) does not refer to u' and v'. The referential trajectory is taken to be the solution of Eqs. (1)–(3) under the given initial and boundary conditions, and the Jacobian is evaluated by substituting the solution into $u^{(0)}$, $v^{(0)}$, $\theta^{(0)}$, $\zeta^{(0)}$ of Eqs. (8)–(10). These equations are simultaneously solved and evolved until the fluctuation of the Lyapunov exponents is sufficiently confined. The extra computation to obtain the first k Lyapunov exponents requires only k times the amount of computational time and storage needed for solving thermal convection fields (Eqs. (1)–(3)), and is acceptable for many practical applications.

When we numerically solve a partial differential equation system the basic equations are often approximated by an ordinary differential equation system whether or not the finite difference method is used. Therefore, the proposed computational method of Lyapunov exponents can be

applied to many numerical solvers of many partial differential equation systems. The present method should be verified by examining the consistency of the computed quantities with the real phenomena as discussed in Section 4.

3. Accuracy assessment

First, the unsteady solution of Eqs. (1)–(3) is compared with a benchmark solution for the case of aspect ratio $\alpha = 8$, $Pr = 0.71$ and $Ra = 3.4 \times 10^5$ [25]. The discretization method, spatial increments $(\Delta x, \Delta y)$, time step (Δt), and convergence criterion are identical with those described in Section 2.1. Results are shown in Tables 1 and 2.

In these tables $\bar{\phi}$, $\tilde{\phi}$ and ϕ_{amp} denote the time-mean value of ϕ, the square root of the volume-mean value of ϕ, and the amplitude of ϕ, respectively. τ_θ denotes the period of the vibration of θ, Nu the averaged Nusselt number on the left hand side wall, k the local kinetic energy $(\boldsymbol{u} \cdot \boldsymbol{u})/2$, and Q the local enstrophy $\zeta^2/2$. These values were evaluated at a referential point $(x, y) = (0.181, 7.370)$ using linear interpolation of the values near the referential point except the volume-mean values. The so-called peak-to-valley amplitude, the difference between the maximum and minimum values, was adopted to evaluate amplitudes.

In Table 1 "Le Quéré" indicates the values of a benchmark solution of Le Quéré computed by a pseudo-spectral method. The fluctuation of computed values by some discretization techniques, including the finite difference method, the finite volume method and the finite element method [25], are shown in "Minimum", "Maximum", "Mean value", and "Standard deviation" rows in Tables 1 and 2. The computed values for this study are shown in the "Ishida et al." row. And the relative differences between the present results and the benchmark results (Table 1) or the above-mentioned mean results (Table 2) are shown in the "Difference" row.

As shown in Table 1 the present study shows good agreement with the benchmark solution by Le Quéré. Though the difference of the amplitudes of u, θ, Nu is relatively large, the difference of the amplitude from the mean value is within the standard deviation computed by some discretization methods, and we can conclude that the results of the present study are accurate enough. For the values shown in Table 2, we cannot compare the present results with the benchmark solution. However the difference of the present study from the mean value is within the standard deviation and such results are good, too.

Moreover we computed $\overline{Nu}$ by using the discretization method described in Section 2.1 for the case of $\alpha = 5$, $Pr = 0.71$ and $Ra = 1.0 \times 10^7$ and found that it agrees well with the value evaluated by the correlation equations proposed by Seki et al. [26] and Churchill and Ozoe [27]. Therefore we can conclude that the spatial increment of the present study is sufficiently small. From these results the present computational methods are ascertained to be accurate enough to analyze the unsteady characteristics of the thermal convection fields for $Ra < 10^7$ and, hereafter, the same computational method was applied for the case of $\alpha = 5$.

4. Results and discussion

4.1. Unsteady characteristics and flow regimes

In this study several reference points were set in the cavity and these points are summarized in Table 3. The amplitude of the vorticity at a reference point (p1) versus Ra is shown in Fig. 2. The figure shows that the vorticity begins to fluctuate at $Ra = 7.3 \times 10^5$, a critical Rayleigh's number

Table 1
Comparison of the present numerical result with other ones including a benchmark solution using a pseudo-spectral method (Le Quéré) [25]

	$\bar{u}$	u_{amp}	θ	θ_{amp}	$\overline{Nu}$	Nu_{amp}	τ_θ
Le Quéré	0.056356	0.054828	0.265480	0.042740	4.57946	0.007100	3.41150
Minimum	0.054000	0.000480	0.244140	0.000260	4.56700	0.000050	3.34640
Maximum	0.065370	0.095000	0.275000	0.072800	9.14500	0.011600	5.05000
Mean value	0.058565	0.061093	0.265301	0.046734	4.73896	0.007692	3.48314
Standard deviation	0.002783	0.016369	0.043795	0.012127	0.83310	0.001982	0.29273
Ishida et al.	0.059032	0.061006	0.265170	0.047639	4.60207	0.008400	3.39994
Difference (%)	4.748	11.269	0.117	11.462	0.494	18.310	0.339

Table 2
Comparison of the present numerical result including volume-averaged properties with other results by using some discretization methods [25]

	$\bar{\psi}$	ψ_{amp}	$\bar{\zeta}$	ζ_{amp}	$\bar{\tilde{k}}$	$(\tilde{k})_{\mathrm{amp}}$	$\bar{\tilde{Q}}$	$(\tilde{Q})_{\mathrm{amp}}$
Minimum	−7.450e−2	5.740e−3	−2.4498	0.9056	0.2373	3.100e−5	2.7020	3.000e−3
Maximum	−5.955e−2	1.160e−2	−1.9914	1.9092	0.2425	7.200e−5	3.0387	4.640e−3
Mean value	−7.249e−2	7.864e−3	−2.2845	1.2325	0.2397	4.093e−5	2.9998	3.488e−3
Standard deviation	3.412e−3	1.675e−3	0.1439	0.3036	9.979e−4	1.216e−5	0.0774	4.266e−4
Ishida et al.	−7.397e−2	7.817e−3	−2.3280	1.2129	0.2396	3.568e−5	3.0062	3.463e−3
Difference (%)	2.042	0.598	1.904	1.589	0.0417	12.832	0.213	0.717

Table 3
Reference points of this study

Reference point	p1	p2	p3	p4	p5
x-coordinate	0.0125	0.025	0.0625	0.5	0.75
y-coordinate	4	0.05	3.75	4.95	1.25

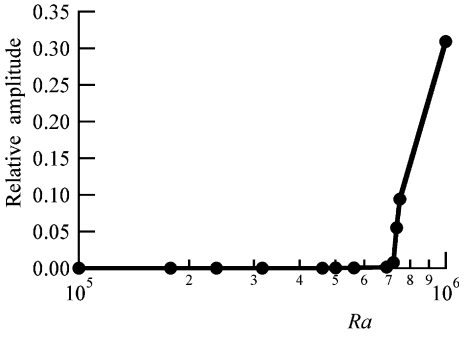

Fig. 2. Relative amplitude of vorticity at reference point (p1). The amplitude is described as the peak-to-valley amplitude of vorticity divided by its time-mean value.

denoted by Ra_{c1}, and after that the thermal fields enter an unsteady state.

Strictly speaking, the computed vorticity shows unsteadiness even when $Ra < Ra_{c1}$. Such a fluctuation is a false or numerical one that is caused by nonzero CC when rounding error is sufficiently small. Fig. 3 shows the variation of the amplitudes of the surface-averaged Nusselt number on the high-temperature side wall Nu, and θ and ζ at the point (p1) as CC is changed. As shown in Fig. 3(b), the amplitudes saturate as CC goes to zero for the case of $Ra > Ra_{c1}$ indicating that the fluctuation makes physical sense. In contrast, for the case of $Ra < Ra_{c1}$, shown in Fig. 3(a), the amplitude goes to zero in a power-law manner with decreasing CC and the fluctuation is determined to be only numerical. This false fluctuation affects the time-variation of the first Lyapunov vector ϕ_1' as described in Section 4.3.

The time traces of the vorticity for $Ra > Ra_{c1}$ at the point (p1) and their power spectrums are shown in Figs. 4 and 5, respectively. As shown in Figs. 4(a) and 5(a) the fluctuation of the vorticity is periodic and indicates that the above-mentioned unsteadiness is caused by the first Hopf bifurcation at $Ra = Ra_{c1}$. For $Ra_{c1} \leqslant Ra < Ra_{c2} \equiv 1.27 \times 10^6$ the fluctuation has a fundamental frequency f_1 along with its harmonics.

For $Ra > Ra_{c2}$ the fluctuation of the vorticity has the components of two fundamental frequencies f_1 and f_2, their (sub-)harmonics and their superpositions, and becomes quasi-periodic as shown in Fig. 5(b)–(d). For the case of $Ra = 1.72 \times 10^6$ and 1.73×10^6 this manner of the superposition is shown precisely in Fig. 6. When Ra is large enough, the spectrum of the fluctuation is continuous and the fluctuation is qualitatively chaotic (Fig. 5(e)). This indicates that the second Hopf bifurcation occurs at $Ra = Ra_{c2}$ and that the transition to chaos follows the Ruelle–Takens scenario. Now it should be noted that the state of $Ra = 1.73 \times 10^6$ cannot be distinguished from that of 1.72×10^6 by power spectrums Fig. 5(c) and (d). In contrast, these states can be clearly and quantitatively distinguished by using the largest Lyapunov exponents.

These results suggest that the thermal convection fields can be classified into four regimes: (a) steady state (S), (b) periodic state (P), (c) quasi-periodic state (QP), and (d) chaotic state (C). However, from the above-described qualitative discussion, the critical Rayleigh number Ra_{c3} between (QP) and (C) cannot be determined and the fluctuation observed in (P) and (QP) cannot be explained or predicted from the unsteady physical quantities in (S) and (P), respectively. This is resolved by using Lyapunov exponents and normalized Lyapunov vectors as discussed below.

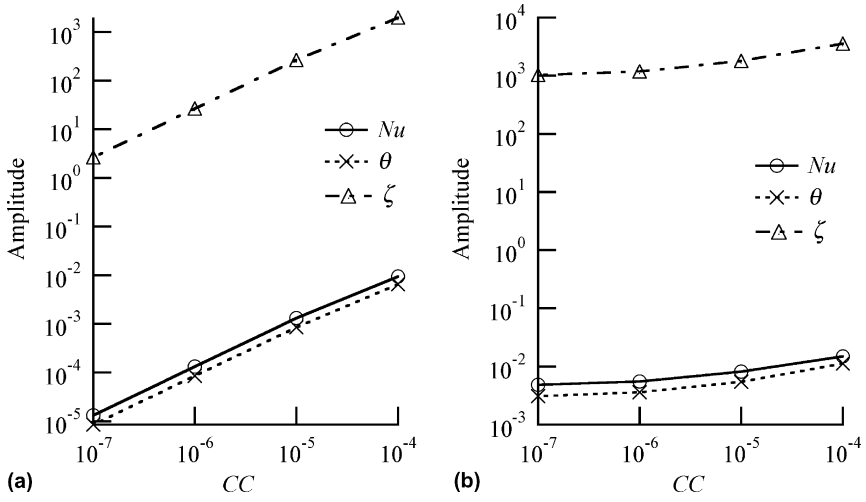

Fig. 3. Variation of some amplitudes versus convergence criterion (CC): (a) $Ra = 5.62 \times 10^5$; (b) $Ra = 7.50 \times 10^5$. Nu is the amplitude of the surface-averaged Nusselt number on the high-temperature side wall. θ and ζ are respectively amplitudes of temperature and vorticity at the reference point (p1).

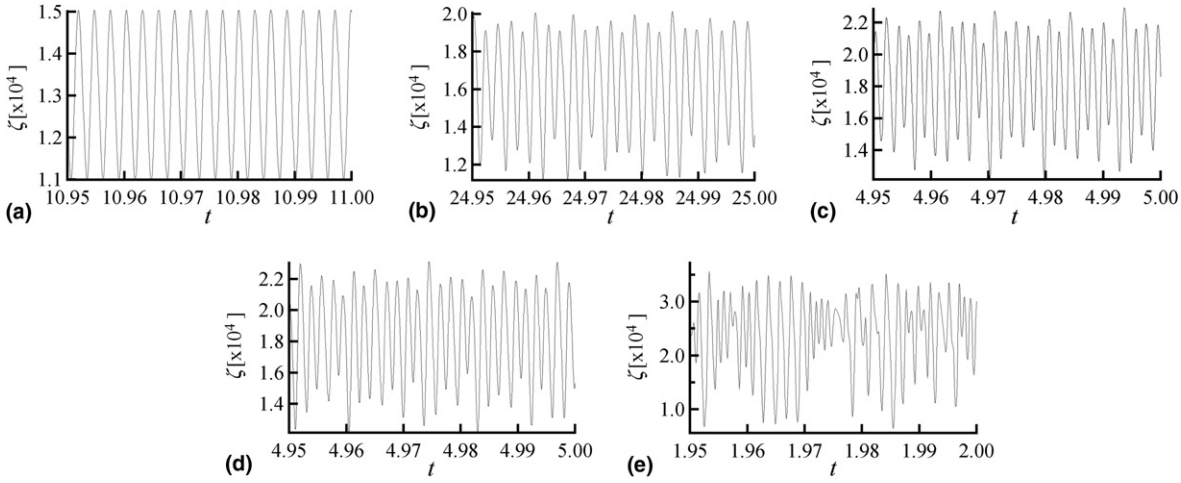

Fig. 4. Time-variation of vorticity at the point (p1) for the same time-range of 0.05: (a) $Ra = 1.00 \times 10^6$; (b) $Ra = 1.43 \times 10^6$; (c) $Ra = 1.72 \times 10^6$; (d) $Ra = 1.73 \times 10^6$; (e) $Ra = 3.16 \times 10^6$.

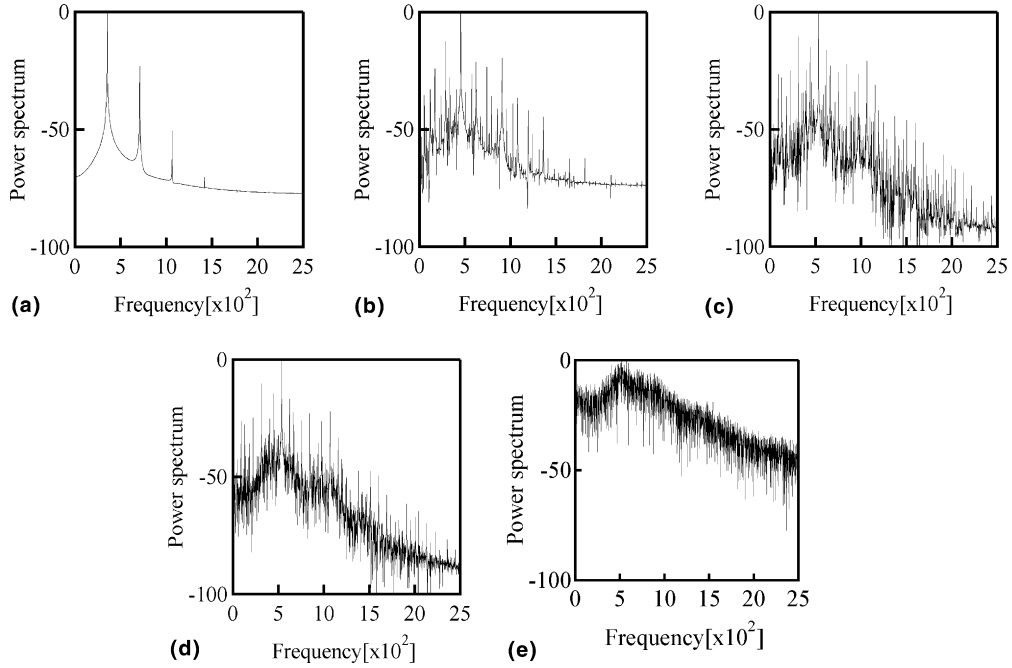

Fig. 5. Power spectrums of vorticity at the point (p1): (a) $Ra = 1.00 \times 10^6$; (b) $Ra = 1.43 \times 10^6$; (c) $Ra = 1.72 \times 10^6$; (d) $Ra = 1.73 \times 10^6$; (e) $Ra = 3.16 \times 10^6$.

4.2. Lyapunov exponents and flow regimes

The largest and second largest Lyapunov exponents versus Ra are shown in Fig. 7. As shown in Fig. 7(c) the largest Lyapunov exponent λ_1 lies in the range of ± 0.5 for $Ra_{c1} = 7.3 \times 10^5 \leqslant Ra \leqslant Ra_{c3} \equiv 1.72 \times 10^6$ and the second largest Lyapunov exponent λ_2 is also included in ± 0.5 for $Ra_{c2} = 1.27 \times 10^6 \leqslant Ra \leqslant Ra_{c3}$. These absolute values are relatively small when compared with the exponents outside the above-mentioned range of Ra. Whether or not the Lyapunov exponents are numerically zero should be decided from the exponents multiplied by the representative time scale for each Ra. In this study we use the following time scale τ for this purpose [28]:

$$\tau \propto \alpha^{1/2} Pr Ra^{-1/2}. \tag{11}$$

From the change in fundamental frequency f_1 against Ra the proportionality constant of τ can be determined to be 1.67 for the present physical model. When the Lyapunov exponents shown in Fig. 7 are expressed in the form of

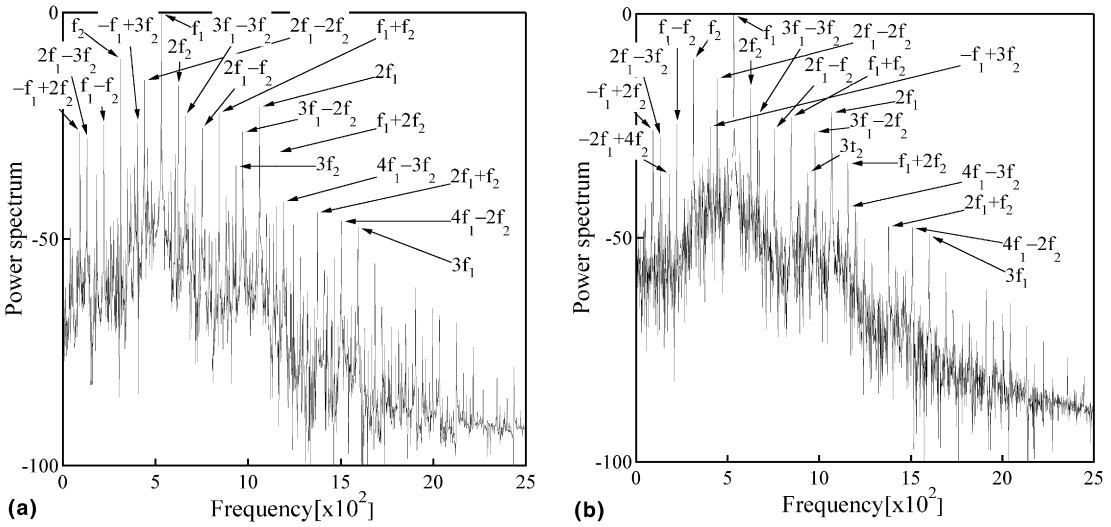

Fig. 6. Closer view of Fig. 5(c) and (d): (a) $Ra = 1.72 \times 10^6$. Fundamental frequencies f_1 and f_2 are 531 and 311, respectively; (b) $Ra = 1.73 \times 10^6$. f_1 and f_2 are 533 and 312, respectively.

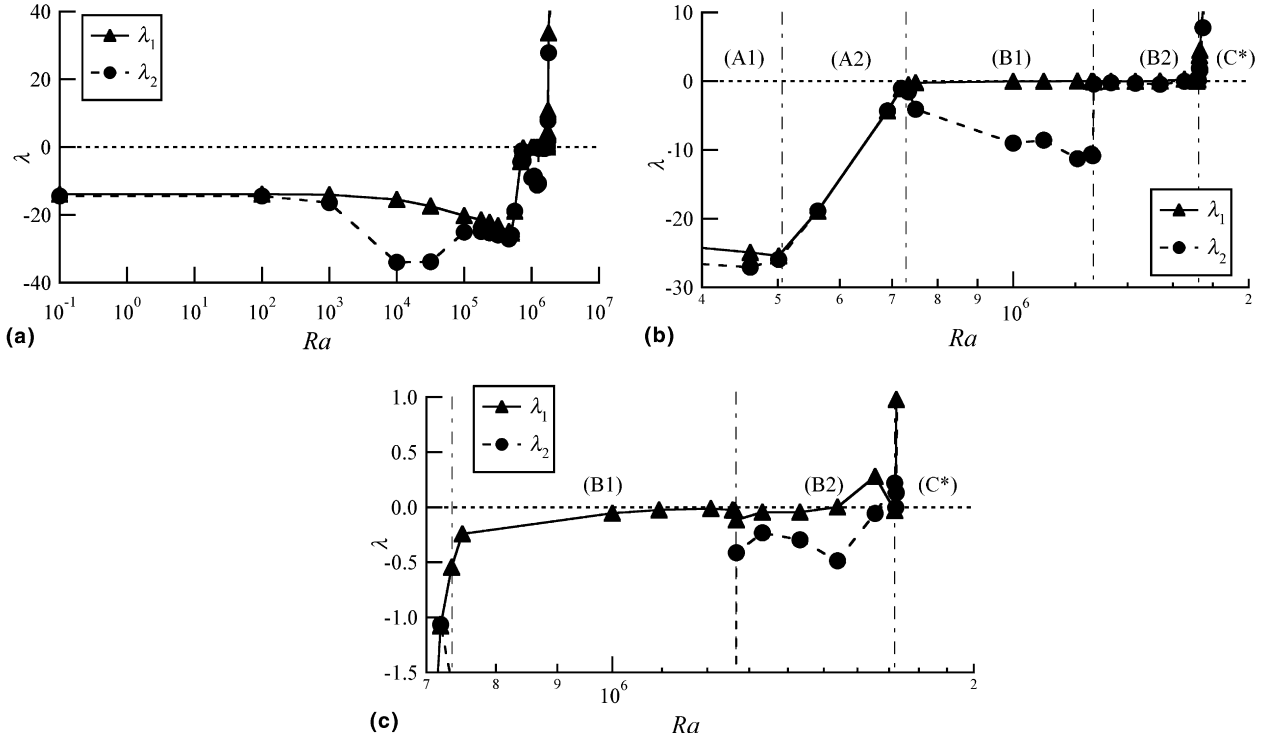

Fig. 7. Variation of the first and second largest Lyapunov exponents for: (a) $0.1 \leqslant Ra \leqslant 1.0 \times 10^7$; (b) $4.0 \times 10^5 \leqslant Ra \leqslant 2.0 \times 10^6$; (c) $7.0 \times 10^5 \leqslant Ra \leqslant 2.0 \times 10^6$. (A1), (A2), (B1), (B2) and (C*) shows the temporal classification of the region of Ra that well explains the characteristics of the exponents.

$\lambda\tau$ the values are the order of 10^{-3} for the above-mentioned range of Ra and the order of 1 outside this range. Therefore the Lyapunov exponents within ± 0.5 described above can be numerically determined to be zero. A similar discussion can be applied to the fact that $\lambda_1 = \lambda_2$ for $Ra_{c0} \equiv 5.0 \times 10^5 \leqslant Ra \leqslant Ra_{c1}$. From these results the thermal convection fields can be classified into the following regions:

(A1) $Ra < Ra_{c0} = 5.0 \times 10^5, \quad \lambda_2 < \lambda_1 < 0,$

(A2) $Ra_{c0} \leqslant Ra < Ra_{c1} = 7.3 \times 10^5, \quad \lambda_2 = \lambda_1 < 0,$

(B1) $Ra_{c1} \leqslant Ra < Ra_{c2} = 1.27 \times 10^6, \quad \lambda_2 \leqslant \lambda_1 = 0,$

(B2) $Ra_{c2} \leqslant Ra \leqslant Ra_{c3} = 1.72 \times 10^6, \quad \lambda_2 = \lambda_1 = 0,$

(C*) $Ra > Ra_{c3}, \quad \lambda_1 > \lambda_2 \geqslant 0.$

Considering only the sign of λ_1, we can divide the thermal convection fields into: region (A) ($\equiv$(A1) + (A2)), region

(B) (≡(B1) + (B2)), and region (C*). In region (A) $\lambda_1 < 0$ and this means that the flow field is stable and in steady state, from the discussion of Section 2.2. This can be ascertained from the fact that region (A) completely corresponds to (*S*) mentioned above. In region (C*) $\lambda_1 > 0$ and, therefore, we conclude that the fields in (C*) are in chaotic state (*C*) from the definition of the largest Lyapunov exponent. So the above-mentioned critical Rayleigh number Ra_{c3} is determined to be 1.72×10^6. It is worthwhile noting that the critical number cannot be obtained from the qualitative discussion in Section 4.1. Similarly the fact that $\lambda_1 = 0$ in region (B) means that the flow fields in the region are periodic or quasi-periodic, and this explains well the real nature of thermal convection fields. However, we cannot divide (B) into the periodic and quasi-periodic regimes from the sign of λ_1 only.

On the other hand, taking λ_2 into consideration we can interpret the five regions mentioned above as follows. The bifurcation from region (A1) to (A2) means that the eigenvalue that has the largest norm changes from a real number to a complex one, and this alludes to the first Hopf bifurcation before λ_1 goes to zero at $Ra = Ra_{c1}$. Similarly the second bifurcation occurs when λ_2 goes to zero, and (B1) and (B2) completely correspond to the regime (*P*) and (QP), respectively. Consequently the thermal convection fields in this study can be classified quantitatively into the following regimes by using λ_1 and λ_2:

$$(\mathrm{A}) \iff (S), \quad (\mathrm{B1}) \iff (P), \quad (\mathrm{B2}) \iff (\mathrm{QP}),$$
$$(\mathrm{C}^*) \iff (C).$$

Rigorously speaking, the Lyapunov exponents computed by Eqs. (6) and (7) fluctuate with time around their time-mean value. The relative width of the error band of λ_1 and λ_2, defined by the peak-to-valley amplitude divided by its time-mean value, was less than 0.9% in (*S*) and the width of λ_2 was less than 3.0% in (*P*). For the case of $|\lambda_i| < 0.5$, the maximum and minimum value of λ_i was included in ±0.55. For some cases, including those in the range (*C*), Eq. (6) or (7) behaves like $\lambda_i + b/(t-a)$ as t increases [20]. In these cases the application of Eqs. (6) and (7) to computation of the exponents is not necessarily effective because it takes too much time to evolve them. In these cases, therefore, λ, a and b were determined by the method of least squares. The fluctuation of the exponents around the correlated curve is relatively large when the evolved time is small. However it is known that such fluctuations make physical sense in statistical mechanics [29] and go to zero when the evolved time is sufficiently large [20].

4.3. Hopf bifurcation and tangent vectors

Since the first and second Lyapunov vectors $\boldsymbol{\phi}'_1$ and $\boldsymbol{\phi}'_2$ have physical meaning as the orthogonalized infinitesimal perturbations included in the system as described in Section 2.2, these perturbations are independently suppressed when λ_1 and λ_2 are negative. Such perturbations independently become obvious over the critical points when λ_1 and λ_2 go to zero, i.e., the first and second Hopf bifurcations, respectively. Therefore the fluctuation of the normalized Lyapunov vector before the critical points can explain the fluctuation of physical quantities over the points. Hereafter the term "Lyapunov vector" is referred to as the normalized vector.

As mentioned above, the largest eigenvalue of the Jacobian (4) changes from a real number to a complex one and, therefore, the first Lyapunov vector begins to fluctuate over the critical point at $Ra = Ra_{c0}$. Fig. 8 shows such a

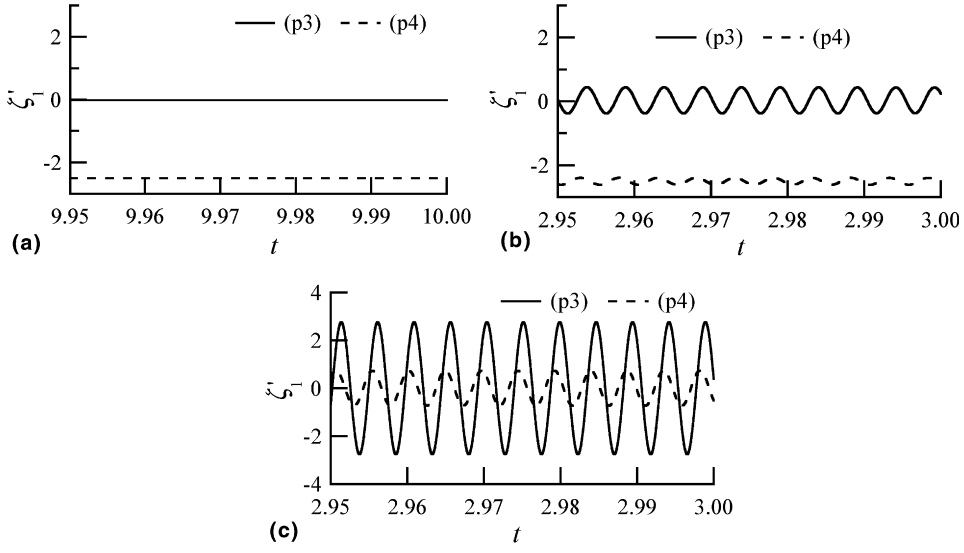

Fig. 8. Time-variation of the vorticity component of the first Lyapunov vector at the reference point (p3) and (p4): (a) $Ra = 4.61 \times 10^5$; (b) $Ra = 5.01 \times 10^5$; (c) $Ra = 5.62 \times 10^5$. The component begins to fluctuate at $Ra_{c0} = 5.0 \times 10^5$.

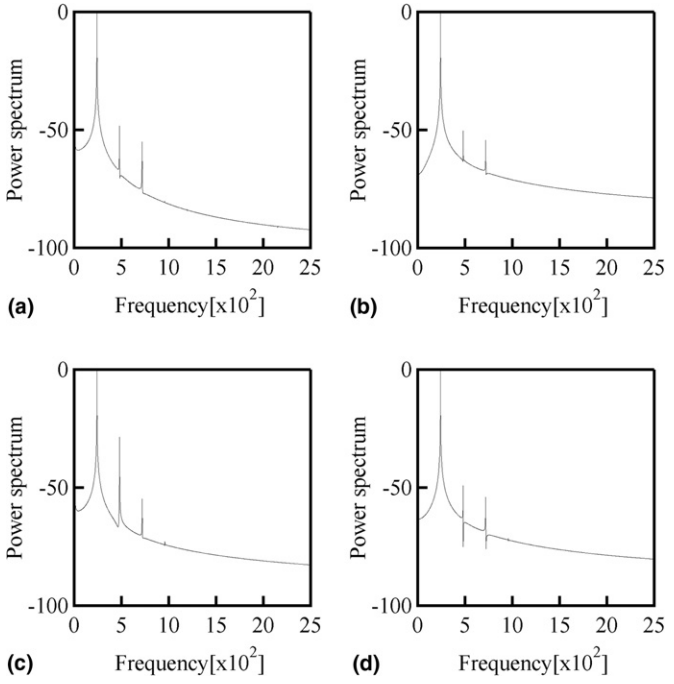

Fig. 9. Power spectrums of the vorticity component of the first Lyapunov vector at $Ra = 7.19 \times 10^5$: (a) (p2); (b) (p3); (c) (p4); (d) (p5). These spectrums have peaks at the same frequency of 239 and its harmonics.

transition of the Lyapunov vector at the reference points (p3) and (p4), described in Table 3.

Fig. 9 shows the power spectrums of the vorticity component of the first Lyapunov vector at the reference points (p2)–(p5) at $Ra = 7.19 \times 10^5 < Ra_{c1}$ below the critical point of the first Hopf bifurcation. These power spectrums have peaks at the same frequency of 239, and well explain the fundamental frequency f_1 of vorticity (=242) at $Ra = Ra_{c1}$. In these spectrums the harmonics of 239 are also detected and this is caused by the false fluctuation described in Section 4.1. Since the Jacobian (4) is fixed in steady state, the corresponding fluctuation of the first Lyapunov vector should be sinusoidal. But the false fluctuation makes the Jacobian (4) periodic and false harmonics are detected in the power spectrums of the Lyapunov vector. However the fluctuation energy of the harmonics is relatively small and the overall fluctuation can be regarded as a sinusoidal one. As mentioned above, the false fluctuation, as well as the false harmonics, can be confined by decreasing CC.

Next, the fluctuation of vorticity at $Ra = Ra_{c1}$ is compared with that of a superpositioned form $\zeta_s + \varepsilon\zeta_1'$ at $Ra = 7.19 \times 10^5 < Ra_{c1}$, where we denote the steady solution by ζ_s, the vorticity component of the first Lyapunov vector by ζ_1, and a proportionality constant by ε. The results are shown in Fig. 10. If we ignore the time-mean and phase shift of the vorticity at each reference point, which is caused by the difference in Ra, then both fluctuations are almost the same. In Fig. 10 the amplitude ε cannot be theoretically obtained because weak nonlinear analyses were not performed in this study. However ε was numerically found to be $\varepsilon \approx 51$ for $Ra = 7.19 \times 10^5$. Such observation is found in Vest and Arpaci [2].

Similarly the fluctuation of vorticity at $Ra = 1.33 \times 10^6$, which is over the critical number Ra_{c2} where the second Hopf bifurcation occurs, was compared with the fluctuation of vorticity and the vorticity component of the second Lyapunov vector at $Ra = 1.26 \times 10^6 < Ra_{c2}$. The power spectrums of these fluctuations are shown in Figs. 11–13. It should be noted that the power spectrum of vorticity at $Ra = 1.33 \times 10^6$, slightly over Ra_{c2}, (Fig. 13) is remark-

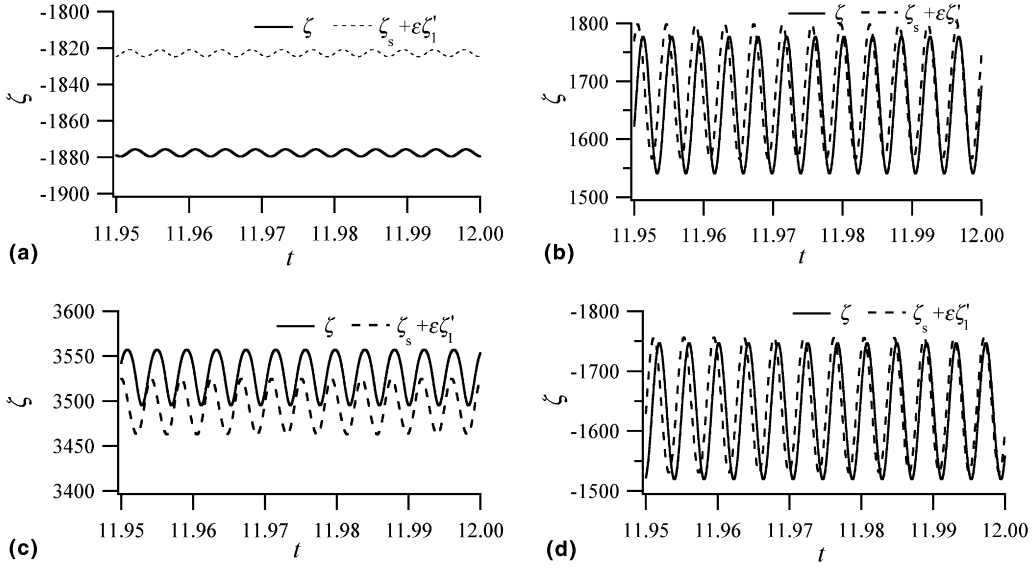

Fig. 10. Comparison of the time-fluctuation of ζ at $Ra_{c1} = 7.3 \times 10^5$ with $\zeta_s + \varepsilon\zeta_1'$ at $Ra = 7.19 \times 10^5 < Ra_{c1}$: (a) (p2); (b) (p3); (c) (p4); (d) (p5). Let ζ denote the vorticity, ζ_s the steady solution, ζ_1 the vorticity component of the first Lyapunov vector, ε a proportionality constant of 51.

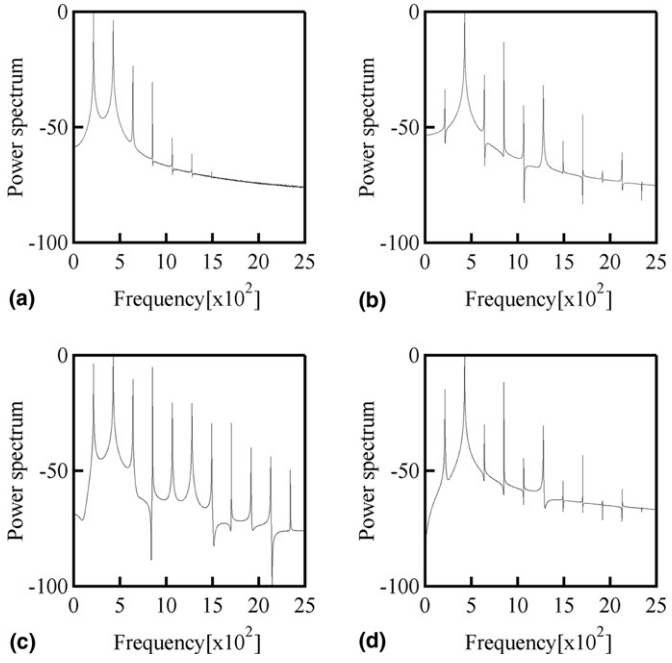

Fig. 11. Power spectrums of the vorticity at $Ra = 1.26 \times 10^6$ for some reference points: (a) (p2); (b) (p3); (c) (p4); (d) (p5).

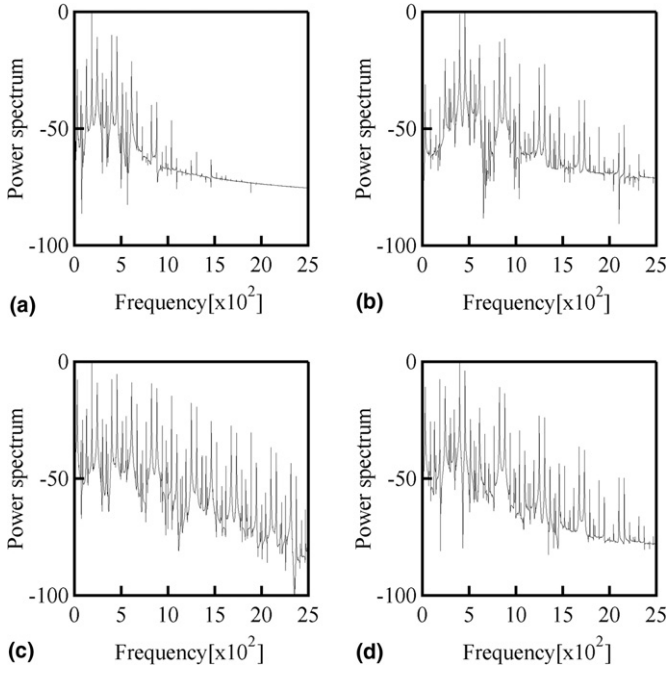

Fig. 12. Power spectrums of the vorticity component of the second Lyapunov vector at $Ra = 1.26 \times 10^6$ for some reference points: (a) (p2); (b) (p3); (c) (p4); (d) (p5).

ably similar to that of the vorticity component of the second Lyapunov vector at $Ra = 1.26 \times 10^6$ (Fig. 12). For reference point (p3) the precise explanation of superposition of fundamental frequencies f_1 and f_2 are shown in Fig. 14. The figure shows that both of the peak frequencies

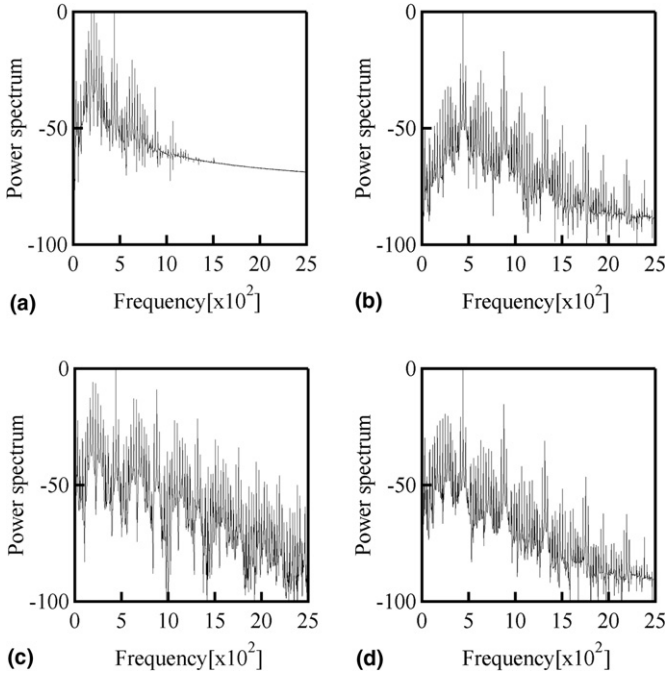

Fig. 13. Power spectrums of the vorticity at $Ra = 1.33 \times 10^6$ for some reference points: (a) (p2); (b) (p3); (c) (p4); (d) (p5).

of vorticity and the vorticity component of the second Lyapunov vector at $Ra = 1.26 \times 10^6$ well explain the frequencies of vorticity at $Ra = 1.33 \times 10^6$. These figures shows that the fluctuation of vorticity at $Ra = 1.33 \times 10^6 > Ra_{c2}$ may be well explained by the fluctuation of vorticity and the vorticity component of the second Lyapunov vector at $1.26 \times 10^6 < Ra_{c2}$ for each point. This is ascertained in Fig. 15. This figure compares the power spectrums of vorticity at $Ra = 1.33 \times 10^6$ (Fig. 13) with that of a superpositioned form $|c_\zeta|^2 + \varepsilon_2^2 |c_{\zeta_2'}|^2$, where c_ζ is the complex form of the Fourier coefficient of vorticity at $Ra = 1.26 \times 10^6$ (Fig. 11), $c_{\zeta_2'}$ is that of the vorticity component of the second Lyapunov vector at the same Ra (Fig. 12), and ε_2 is a proportionality constant of 0.45. As shown in Figs. 11, 12 and 14, the major frequency of vorticity differs from that of the vorticity component of the second Lyapunov vector at $Ra = 1.26 \times 10^6$ and, therefore, the contribution of the product $c_\zeta \cdot c_{\zeta_2'}$ to the power spectrum can be ignored and is neglected in Fig. 15. Fig. 15(a)–(d) show that major vibration components over -60 dB at $Ra = 1.33 \times 10^6 > Ra_{c2}$ (except the direct current component) are quantitatively explained by the fluctuation of vorticity superpositioned on the fluctuation of the vorticity component of the second Lyapunov vector at $Ra = 1.26 \times 10^6 < Ra_{c2}$. From these results we can conclude that the fluctuation of a physical quantity and its component of the second Lyapunov vector slightly under the critical point Ra_{c2} at which the second Hopf bifurcation occurs well explain the fluctuation of the physical quantity just over the critical point.

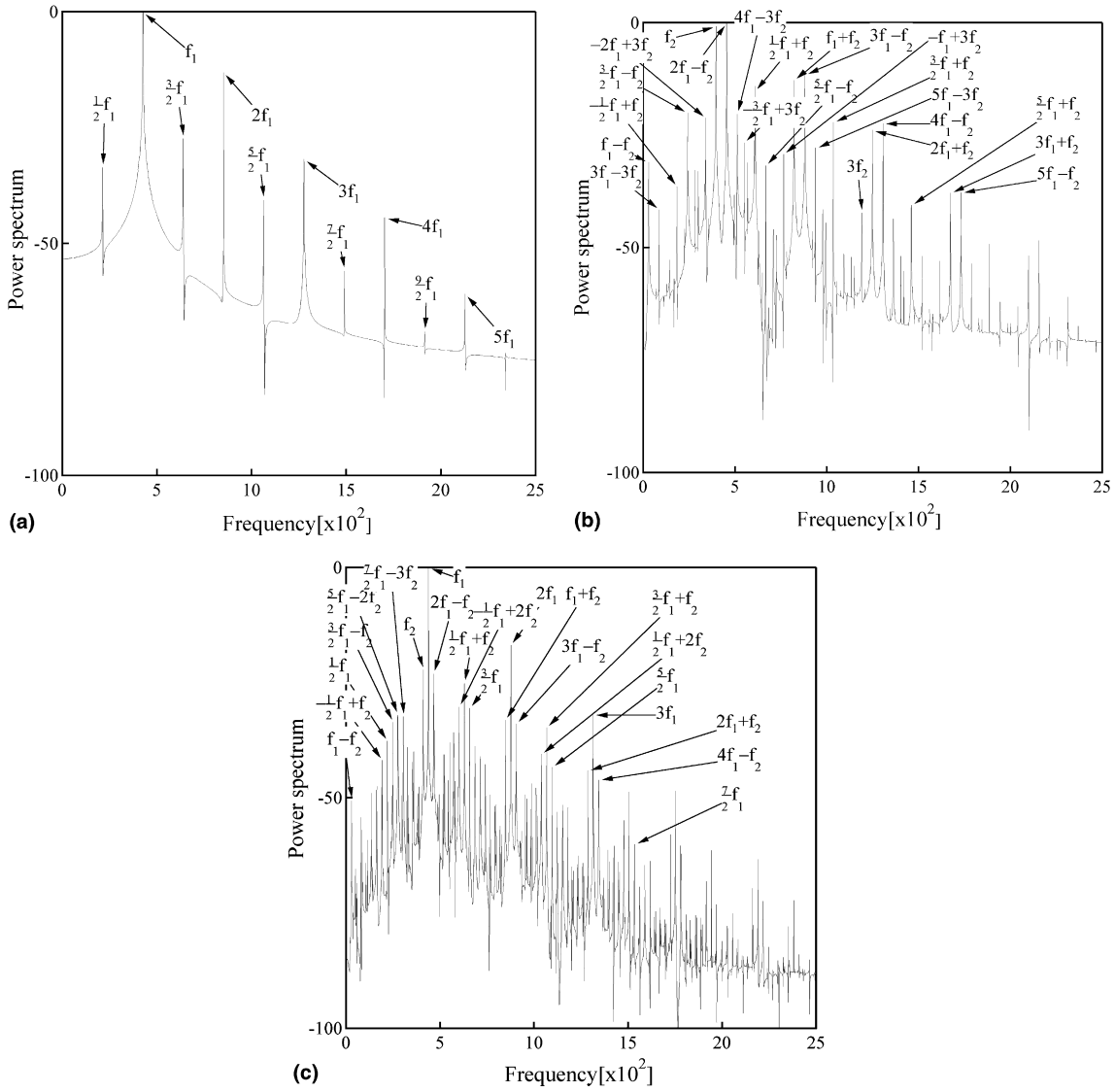

Fig. 14. Closer view of the power spectrums at the point (p3) (Figs. 11(b), 12(b) and 13(b)): (a) vorticity at $Ra = 1.26 \times 10^6$ ($f_1 = 425$); (b) vorticity component of the second Lyapunov vector at $Ra = 1.26 \times 10^6$ ($f_1 = 425$, $f_2 = 397$); (c) vorticity at $Ra = 1.33 \times 10^6$ ($f_1 = 438$, $f_2 = 410$).

5. Conclusions

In this study we have proposed an accurate and simple method to evaluate the Lyapunov spectrum. The method is suitable for any discretization method that finally expresses a governing equation system in the form of an ordinary differential equation system. The method was applied to evaluate the first and second largest Lyapunov exponents for the natural convection in a rectangular cavity with heated and cooled side walls. The main results are as follows:

(1) The largest and second largest Lyapunov exponents can be evaluated using the proposed method without any parameters that affect the exponents. The method just requires several times the amount of computational time and storage than the conventional thermal convection fields and is useful for many applications.

(2) The second largest Lyapunov exponent makes it possible to classify quantitatively thermal convection fields into five regimes against the Rayleigh number and to clarify the transition route from steady state to chaos by identifying the first and second Hopf bifurcations. These analyses cannot be done without the exponent. The exponent, as well as the largest Lyapunov exponent, provides a unified measure to analyze the change of flow regimes.

(3) The fluctuation of thermal convection fields slightly over the critical Rayleigh number at which Hopf bifurcation occurs can be explained quantitatively from the corresponding physical quantity and its component of normalized Lyapunov vector, associated with the computation of the Lyapunov exponents, slightly under the critical point.

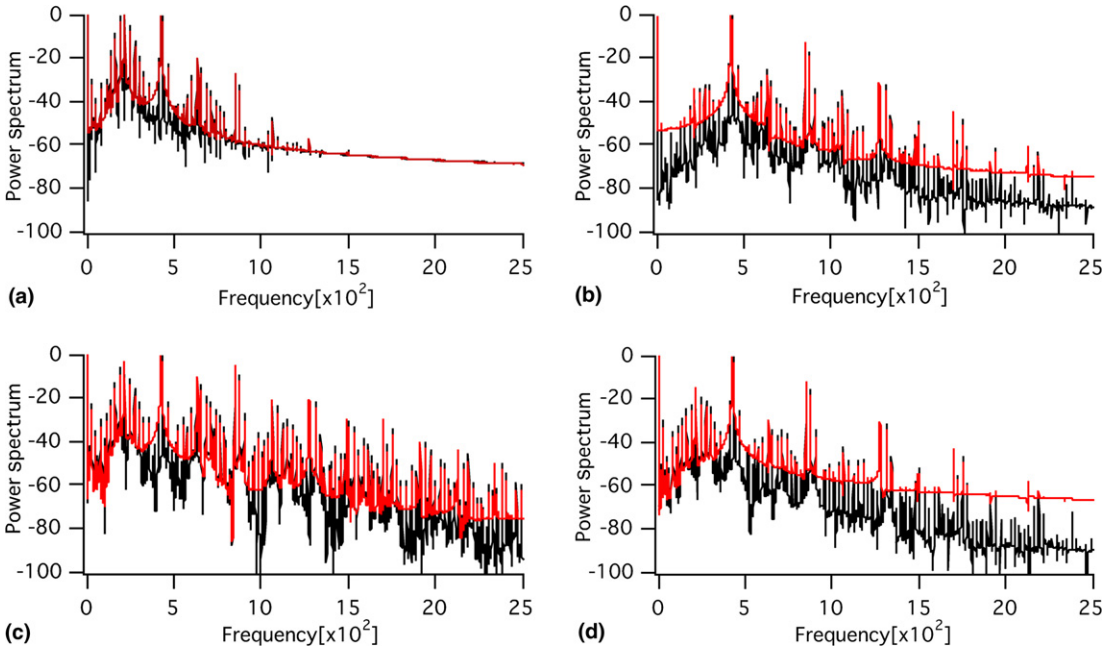

Fig. 15. Comparison of the power spectrums of vorticity at $Ra = 1.33 \times 10^6$ (black solid line) with $|c_\zeta|^2 + \varepsilon_2^2|c_{\zeta_2'}|^2$ (red solid line) at some reference points, where c_ζ is the complex form of the Fourier coefficient of vorticity at $Ra = 1.26 \times 10^6$, $c_{\zeta_2'}$ is that of the vorticity component of the second Lyapunov vector at the same Ra, and ε_2 is a proportionality constant of 0.45: (a) (p2); (b) (p3); (c) (p4); (d) (p5). (For interpretation of references in color, the reader is referred to the web version of this article.)

The relationships between chaotic and turbulent flows are important though it is not discussed in this study. If we consider "turbulence" as the complex flow regime where the flow has self-similar vortex structures and large discrepancy between the spatial scales of time-averaged kinetic energy input and output (dissipation), the chaotic flow of the present study ($Ra < 10^7$) has far smaller chaotic degrees of freedom and does not correspond to such turbulent flow. However, the correspondence may not be independent of the quantitative definition of turbulent flow. Various indicators of chaotic dynamics, such as Lyapunov exponents, can contribute to the definition. Moreover, how the three dimensionality of chaotic (turbulent) flow or discretization methods of basic equations affect the above-mentioned chaotic characteristics remains an unsettled problem. It is an issue for the future.

Acknowledgements

We would like to thank Prof. N. Sugimoto for his comments on Lyapunov exponents. This research was partially supported by the Japan Society for the Promotion of Science, Grant-in-Aid for Encouragement of Young Scientists (B), No. 15760132.

References

[1] J. Mizushima, Y. Hara, Routes to unicellular convection in a tilted rectangular cavity, J. Phys. Soc. Jpn. 69 (2000) 2371–2374.
[2] C.M. Vest, V.S. Arpaci, Stability of natural convection in a vertical slot, J. Fluid Mech. 36 (1969) 1–15.
[3] S.A. Suslov, S. Paolucci, Nonlinear analysis of convection flow in a tall vertical enclosure under non-Boussinesq conditions, J. Fluid Mech. 344 (1997) 1–41.
[4] J. Mizushima, H. Tanaka, Transition routes of natural convection in a vertical fluid layer, J. Phys. Soc. Jpn. 71 (2002) 2898–2906.
[5] S. Xin, P. Le Quéré, Direct numerical simulations of two-dimensional chaotic natural convection in a differentially heated cavity of aspect ratio 4, J. Fluid Mech. 304 (1995) 87–118.
[6] S. Wakitani, Formation of cells in natural convection in a vertical slot at large Prandtl number, J. Fluid. Mech. 314 (1996) 299–314.
[7] S. Paolucci, D.R. Chenoweth, Transition to chaos in a differentially heated vertical cavity, J. Fluid Mech. 201 (1989) 379–410.
[8] P. Le Quéré, M. Behnia, From onset of unsteadiness to chaos in a differentially heated square cavity, J. Fluid Mech. 359 (1998) 81–107.
[9] H. Ishida, K. Kure, H. Kimoto, Quasi-static and chaotic characteristics of the natural convection field in a vertical slot, Heat Trans.—Asian Res. 30 (2001) 40–53.
[10] H. Ishida, T. Yamashita, H. Kimoto, Stability and chaotic characteristics of a wall plume, Int. J. Heat Mass Transfer 45 (2002) 3471–3476.
[11] H. Ishida, H. Kimoto, The structure of attractors reconstructed with time-evolution data of average heat transfer on thermal convection field in a vibrating square enclosure, Heat Trans.—Asian Res. 30 (2001) 11–21.
[12] A. Wolf, J.B. Swift, H.L. Swinney, J.A. Vastano, Determining Lyapunov exponents from a time series, Physica D 16 (1985) 285–317.
[13] F. Takens, Detecting strange attractors in turbulence, in: D.A. Rand, L.-S. Young (Eds.), Lecture Note in Mathematics, vol. 898, Springer, Berlin, 1981, pp. 366–381.
[14] C.-H. Bruneau, M. Saad, From a steady to chaotic solutions in a differentially heated cavity of aspect ratio 8, Int. J. Numer. Meth. Fluids 40 (2002) 1093–1107.
[15] J. Kaplan, J. Yorke, Functional differential equations and approximation of fixed points, in: H.O. Peitgen, H.O. Walther (Eds.), Lecture Note in Mathematics, vol. 730, Springer, Berlin, 1979, p. 228.
[16] Y. Pesin, Characteristic Lyapunov exponents and smooth ergodic theory, Russ. Math. Surveys 32 (1977) 55–114.

[17] M. Sano, Y. Sawada, Measurement of the Lyapunov spectrum from a chaotic time series, Phys. Rev. Lett. 55 (1985) 1082–1085.
[18] G. Bennetin, L. Galgani, J.-M. Strelcyn, Kolmogorov entropy and numerical experiments, Phys. Rev. A 14 (1976) 2338–2345.
[19] I. Shimada, T. Nagashima, A numerical approach to ergodic problem of dissipative dynamical systems, Prog. Theor. Phys. 61 (1979) 1605–1616.
[20] I. Goldhirsh, P.-L. Sulem, S.A. Orszag, Stability and Lyapunov stability of dynamical systems: a differential approach and a numerical method, Physica D 27 (1987) 311–337.
[21] J. Lu, G. Yang, H. Oh, A.C.J. Luo, Computing Lyapunov exponents of continuous dynamical systems: method of Lyapunov vectors, Chaos, Soliton Fractals 23 (2005) 1879–1892.
[22] J.R. Dorfman, An Introduction to Chaos in Nonequilibrium Statistical Mechanics, Cambridge University Press, 1999, pp. 100–104.
[23] R. Seydel, Practical Bifurcation and Stability Analysis, second ed., Springer-Verlag, 1994, pp. 261–262.
[24] G.H. Golub, C.F. Van Loan, Matrix Computations, third ed., The Johns Hopkins University Press, 1996, pp. 330–332.
[25] M.A. Christon, P.M. Gresho, S.B. Sutton, Computational predictability of time-dependent natural convection flows in enclosures (including a benchmark solution), Int. J. Numer. Meth. Fluids 40 (2002) 953–980.
[26] N. Seki, S. Fukusako, H. Inaba, Visual observation of natural convection flow in a narrow vertical cavity, J. Fluid Mech. 84 (1978) 695–704.
[27] S.W. Churchill, Free convection in layers and enclosures, Heat Exchanger Design Handbook, Hemispher Publishing Co., New York, 1983, 2.5.8.
[28] J. Patterson, J. Imberger, Unsteady natural convection in a rectangular cavity, J. Fluid Mech. 100 (1980) 65–86.
[29] H. Fujisaka, Statistical dynamics generated by fluctuations of local Lyapunov exponents, Prog. Theor. Phys. 70 (1983) 1264–1275.